



Long-life Graphite – Lithium Sulfide Full Cells Enabled through a Solvent Co-intercalation-free Electrolyte Design

Journal:	Materials Horizons
Manuscript ID	MH-COM-09-2024-001287.R1
Article Type:	Communication
Date Submitted by the Author:	04-Nov-2024
Complete List of Authors:	Lai, Tianxing; The University of Texas at Austin Bhargav, Amruth; The University of Texas at Austin Reed, Seth; The University of Texas at Austin Manthiram, Arumugam; The University of Texas at Austin, Materials Science and Engineering

SCHOLARONE™ Manuscripts

New Concepts

We introduce a novel electrolyte design for lithium-sulfur (Li-S) batteries that enables the use of graphite (Gr) anodes instead of lithium metal. By replacing 1,2-dimethoxyethane (DME) with 1,1,2,2-tetrafluoroethyl 2,2,3,3-tetrafluoropropylether (TTE) in the conventional 1,3-dioxolane (DOL)/DME electrolyte, without changing the salt concentration, we achieve significant improvements in anode compatibility. Unlike the DOL/DME electrolyte, the DOL/TTE electrolyte effectively suppresses solvent co-intercalation and reduction, thereby enhancing Gr anode stability. Our study also reveals that gas evolution, closely linked to solvent co-intercalation and electrolyte decomposition, is significantly mitigated by the DOL/TTE formulation. This approach is different from strategies like ether-based localized high concentration electrolytes (LHCEs), as it maintains sulfur cathode kinetics with minimal interference. More importantly, the use of Gr anodes circumvents the instability and poor reversibility associated with Li-metal anodes. Both lithiated-Gr | | S and Gr | Li₂S configurations are demonstrated to have stable long-term cycling performance with a negative-to-positive capacity (N/P) ratio of 1.5 and 1.05, respectively, which is not feasible with Li-metal anodes. This electrolyte design concept provides a practical route to overcoming the key limitations in Li-S batteries development, advancing their viability as the next-generation high-energy-density batteries.

COMMUNICATION

Long-life Graphite – Lithium Sulfide Full Cells Enabled through a Solvent Co-intercalation-free Electrolyte Design

Tianxing Lai, ^a Amruth Bhargav, ^a Seth Reed, ^a and Arumugam Manthiram *^a

Received 00th January 20xx, Accepted 00th January 20xx

DOI: 10.1039/x0xx00000x

Graphite (Gr) is the predominant anode material for current lithium-ion technologies. Gr anode could offer a practical pathway for the development of lithium-sulfur (Li-S) batteries due to its superior stability and safety compared to Li-metal. However, Granodes are not compatible with the conventional dilute ether-based electrolytes typically used in Li-S systems. Here, an optimized ether electrolyte is presented, utilizing 1 M lithium bis(trifluoromethanesulfonyl)-imide (LiTFSI) in 1,3dioxolane (DOL) 1 1,1,2,2-tetrafluoroethyl 2,2,3,3tetrafluoropropylether (TTE). Without altering the salt concentration, this electrolyte regulates the solvation structure and promotes the formation of a robust solidelectrolyte interphase (SEI) layer, leading to a significant improvement in the cyclability of Gr anodes. Meanwhile, the DOL/TTE electrolyte maintains adequate kinetics for the sulfur cathode, enabling its pairing with Gr anodes without any cathode modification. The cell with a Gr anode delivers a reversible discharge capacity of 515 mA h g-1 after 400 cycles at C/10 rate, in contrast to only 143 mA h g-1 for the Li-metal anode cell. Moreover, a Gr || Li₂S full cell with a negative-topositive capacity (N/P) ratio of 1.05 and a Li₂S loading of 3 mg cm⁻² shows a stable 58% capacity retention after 400 cycles.

1. Introduction

Lithium-sulfur (Li-S) batteries have emerged as a promising alternative to current lithium-ion (Li-ion) technologies, offering a high theoretical energy density (2,600 W h kg $^{-1}$) and the potential for lowering the cost due to the abundance of sulfur. However, the practical implementation of Li-S batteries faces significant challenges related to both the

Regulating the characteristic of the SEI layer and Li deposition behaviors is critical for addressing these issues. 16,17 Naturally, the electrolyte, as the component in direct contact with the anode, plays an important role in protecting the Li anode and has attracted much attention recently in the research community. Novel electrolyte designs, particularly high-concentration electrolytes (HCEs) and localized high-concentration electrolytes (LHCEs), have emerged as effective strategies to enhance the cyclability of Li-metal anode. 18-20 They enable the formation of a stable SEI and can limit the detrimental side reactions between Li metal and electrolyte components. 21 Meanwhile, in a Li-S system, they have the potential to limit LiPS from shuttling to the anode. 22-25 However, the ultra-low solubility of LiPS in HCEs and LHCEs leads to extremely sluggish sulfur

commercialization of Li-S batteries.

DOI: 10.1039/x0xx00000x

anode and cathode. At the sulfur cathode, the sulfur redox kinetics is sluggish, mainly due to the low electronic and ionic conductivities of elemental sulfur and its end discharge product Li₂S. Meanwhile, at the Li metal anode, the formation of an unstable solid electrolyte interphase (SEI) leads to electrolyte depletion, low Li plating and stripping efficiencies, and Li dendrite growth, which can further result in cell failure and safety issues.² Additionally, lithium polysulfides (LiPS), as an electrolyte soluble intermediate during cycling, shuttle between the electrodes, causing active material loss and Li-metal degradation.3 In recent years, numerous strategies have been proposed to enhance the sulfur redox kinetics, including the use of nanostructured hosts and catalytic materials.4-12 The performance of sulfur cathodes has thus been significantly improved. Nevertheless, there are relatively fewer effective approaches reported to extend the service life of Li-metal anode in Li-S systems, especially under practical cell parameters. 13-15 The inability to stabilize the Li anode remains one of the major challenges for

^a Materials Science & Engineering Program and Texas Materials Institute, The University of Texas at Austin, Austin, TX, 78712 USA. E-mail: rmanth@mail.utexas.edu

[†] Electronic supplementary Information (ESI) available. See

conversion kinetics, which limits their practical viability in LiS cells.

Another possible approach to mitigate the anode-related issues in Li-S batteries is to replace the Li-metal anode with a more stable alternative, such as graphite (Gr) or siliconbased anodes. These anode materials function through an insertion or alloying mechanism, having much better control over Li dendrite growth. Additionally, they are generally easier and safer to handle compared to Li metal, as they are less reactive. Gr and Si/Gr anodes have been successfully employed in current Li-ion batteries with layered oxide cathodes. However, when utilizing them in a Li-S system, the choice of electrolyte becomes again important. Carbonate-based electrolytes, as the conventional electrolytes for Gr and Si/Gr anodes, are usually not compatible with sulfur cathodes. The nucleophilic

polysulfide anion can attack the carbonate solvent, leading to solvent decomposition and active material loss.³¹ Moreover, the commonly used 1,3-dioxolane (DOL) / 1,2-dimethoxyethane (DME)-based electrolyte for Li-S cells also exhibits instability when paired with Gr anodes, due to the solvent co-intercalation effect.³² A few electrolyte designs have been proposed to enable the performance of Gr anodes in Li-S systems.³³⁻³⁸ Nevertheless, most of the designs rely on the use of HCEs or LHCEs, which compromise the kinetics of sulfur cathodes and reduce the overall energy density of the cell. Moreover, the properties and behaviors of Gr anodes in such systems need to be more carefully investigated.

In this work, an ether-based electrolyte consisting of 1 M lithium bis(trifluoromethanesulfonyl)imide (LiTFSI) in DOL / 1,1,2,2-tetrafluoroethyl 2,2,3,3-tetrafluoropropylether (TTE)

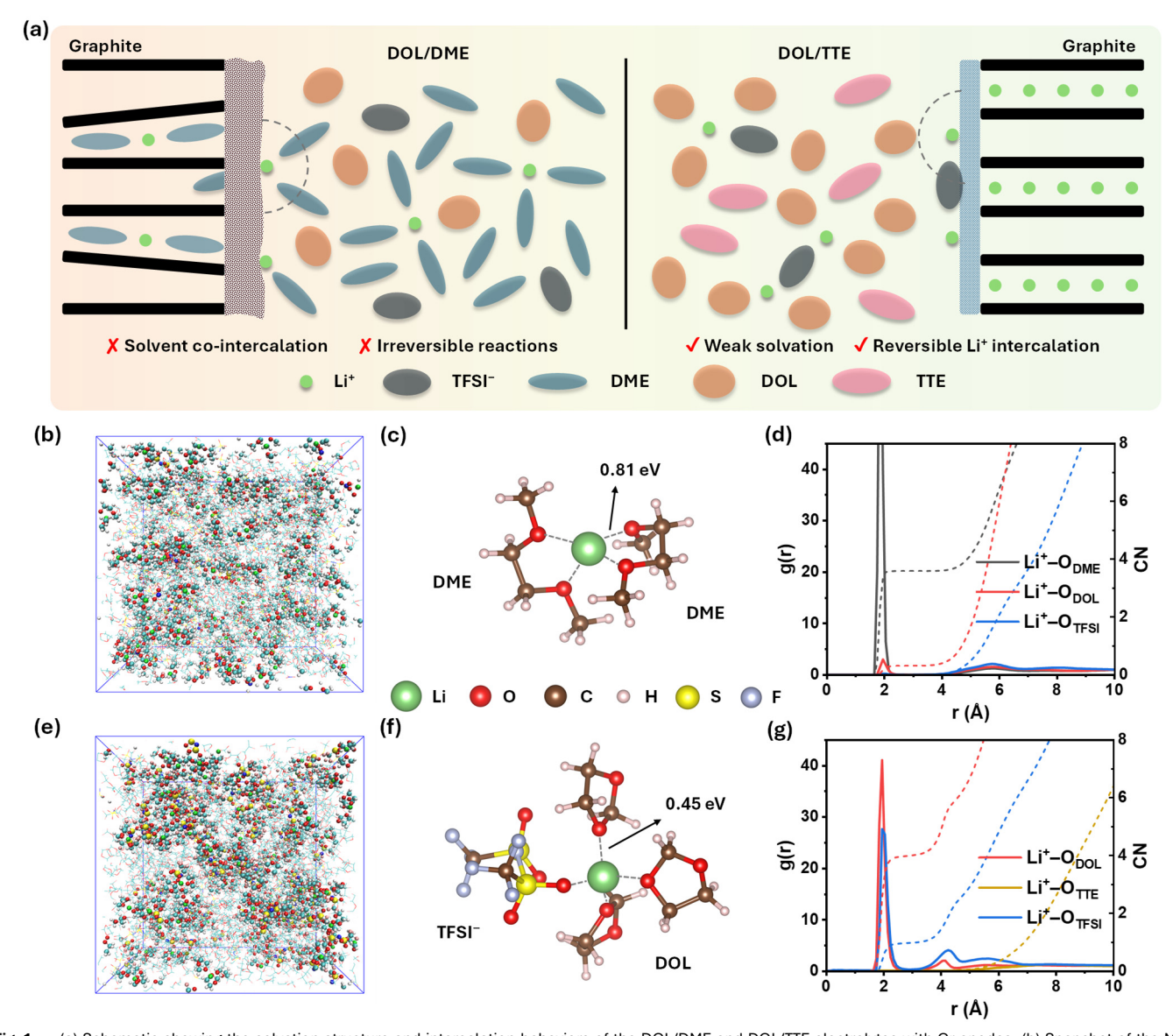


Fig. 1 (a) Schematic showing the solvation structure and intercalation behaviors of the DOL/DME and DOL/TTE electrolytes with Gr anodes. (b) Snapshot of the MD simulation cell for the DOL/DME electrolyte. (c) Representative Li* solvation structure, (d) RDF and coordination number derived from the MD results for the DOL/DME electrolyte. The Li* solvation structure is determined by species within 0.3 nm of Li*. (e) Snapshot of the MD simulation cell for the DOL/TTE electrolyte. (f) Representative Li* solvation structure and (g) RDF and coordination number for the DOL/TTE electrolyte.

Materials Horizons COMMUNICATION

is designed to stabilize the Gr anode in the Li-S system. By replacing DME with TTE in the conventional DOL/DME electrolyte, the solvation structure is effectively modulated to improve the compatibility of the electrolyte to Gr anode. The structural change and surface chemistry of the Gr anode utilizing the DOL/TTE electrolyte are carefully studied with various techniques. We demonstrate that the solvent cointercalation and decomposition in Gr anode are effectively inhibited with this electrolyte, promoting the generation of a robust SEI layer; thus, the cyclability of Gr anode is significantly improved in the ether electrolyte. Additionally, Gr anode is proven to generate less gases from solvent and salt decomposition when cycling in the DOL/TTE electrolyte. This electrolyte unlocks the potential of Gr anode when pairing with a sulfur cathode, exhibiting better cyclability compared to Li-metal anode, even with a limited excess of Li and without any cathode modification. Furthermore, a Gr || Li₂S full cell (without the need for pre-lithiation) with a negative-to-positive capacity (N/P) ratio of 1.05 and a Li₂S loading of 3 mg cm⁻² shows stable long-term cyclability over 400 cycles. This work demonstrates the potential of Gr anodes in Li-S batteries with ether-based electrolytes and highlights their working mechanism, offering a pathway for their practical application.

2. Results and Discussion

Fig. 1a reveals the logic and the potential functioning mechanism of the DOL/TTE electrolyte. The conventional 1 M LiTFSI in DOL/DME (v/v = 1:1) electrolyte with LiNO₃ additive shows acceptable performance in Li-S batteries due to its high ionic conductivity, good compatibility with Li metal, and reasonable control over LiPS shuttling. However, the flexibility of the linear DME molecule and its two coordinating O atoms make the Li⁺ solvation structure quite stable, thereby having a high de-solvation energy for Li⁺ (Fig. S1).^{39,40} When it comes to the case of Gr anode, this can lead to intercalation of the entire solvation structure as the solvent molecules are hard to detach from Li+, causing poor performance and potential cell failure. On the other hand, DOL features moderate solvating power due to the steric hindrance imposed by its cyclic structure. Therefore, we eliminate DME from the system and utilize DOL as the major solvating solvent, hoping to minimize the solvent cointercalation at the anode. Meanwhile, a non-solvating solvent TTE is introduced into the electrolyte to further tune the solvation environment of Li⁺ and control the solubility of LiPS (Fig. S2). The Raman spectrum of the TFSI- vibration mode shows a blueshift from 742 $\mbox{cm}^{\mbox{-}1}$ in the DOL/DME electrolyte to 746 cm⁻¹ in the DOL/TTE electrolyte (Fig. S3), indicating the formation of more contact-ion pairs (CIPs) and aggregates (AGGs).41,42 Noting that the salt concentration and solvent ratio remain the same in the DOL/TTE electrolyte (1 M and v/v = 1), therefore the change in solvation structure is not as obvious as in LHCEs, where the solvation structure may predominantly be AGGs; however, the DOL/TTE

electrolyte still makes significant difference in performance, and is arguably more suitable for Gr-Li2S cells.

The change in the local solvation environment is further studied with molecular dynamics (MD) simulations (Fig. 1b and e). Statistic data show that the dominant Li⁺ solvation structure in the DOL/DME electrolyte is 1 Li⁺ with 2 DME, making it four oxygen coordinated due to the chelating effect of DME (Fig. 1c and d). In contrast, in the DOL/TTE electrolyte, TFSI $^{\scriptscriptstyle{-}}$ enters the solvation shell of Li $^{\scriptscriptstyle{+}}$ along with three DOL molecules, matching well with the Raman results (Fig. 1f and g). This can also be observed in the radial distribution functions (RDFs) and the corresponding coordination number. A sharp peak of Li⁺-O_{TFSI} appears in the RDF plot for the DOL/TTE electrolyte, corresponding to a coordination number of ~ 1 for the pairing O atoms. Further calculations by density functional theory (DFT) show that each DOL molecule has a binding energy of 0.45 eV with the remaining solvation structure, contrasting 0.81 eV for each DME molecule in the DME/DOL electrolyte. This indicates that Li* would have a lower desolvation barrier at the anode interphase in the DOL/TTE electrolyte, which is beneficial for suppressing solvent co-intercalation.

Li || Gr half cells were assembled to assess the compatibility of Gr anode with DOL/DME and DOL/TTE electrolytes. As shown in Fig. 2a, the DOL/DME cell exhibits a specific capacity of 460 mA h g⁻¹ during the initial discharge, which is higher than the theoretical lithiation capacity for graphite. It should be noted that the cell got roughly half of the discharge capacity before 0.25 V, while Li⁺ intercalation usually happens below 0.25 V. Moreover, during the first charge step, only 15.8% (72.9 mA h g⁻¹) of the capacity was recovered, indicating severe and irreversible side reactions occurring during discharge. The DOL/TTE cell, on the other hand, shows stable multistep discharge voltage plateaus below 0.25 V, a specific capacity of 356 mA h g⁻¹, and a high initial Columbic efficiency (CE) of 91%. This also warrants stable cycling of the cell, delivering a capacity of 335 mA h g ¹ after 50 cycles with a high CE (99.7% in average at C/5), compared to only 16.1 mA h g-1 for the DOL/DME cell (Fig. 2b and Fig. S4). To make a more comprehensive comparison, a DOL/DME electrolyte that does not have LiNO3 was also evaluated. The cell shows even worse performance than the regular DOL/DME electrolyte. This could result from the influence of LiNO₃ on the solvation structure and improvement in the SEI layer. 43,44

The different behavior of Gr was also confirmed by cyclic voltammetry (CV). The CV curves of the DOL/DME cell display multiple peaks between 0.3 and 1 V at the first cycle, corresponding to irreversible Li*-solvent co-intercalation, followed by solvent reduction (Fig. S5). ^{39,45} In the following cycles, the response current keeps decreasing, suggesting continuous detrimental reactions in the cell. In contrast, the DOL/TTE electrolyte is able to stabilize the Gr anode, showing only redox peaks for Li* intercalation with significantly higher response current. After the initial activation, the succeeding CV curves are overlapping, demonstrating a stable and reversible Li* intercalation with

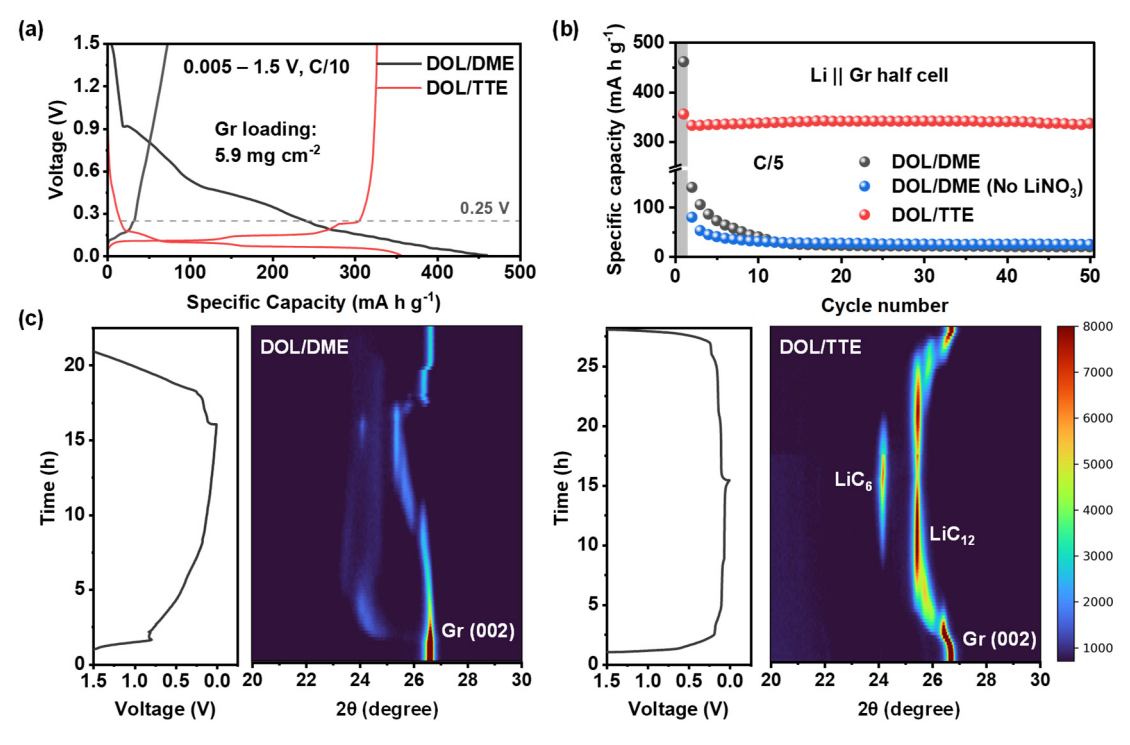


Fig. 2 (a) Voltage profiles of Li || Gr cells with different electrolytes during the 1st formation cycle at C/10 rate. (b) Cycling performance of Li || Gr cells with different electrolytes at C/5 rate (with one formation cycle at C/10). Operando XRD measurements of Li || Gr cells with different electrolytes for one cycle at C/15 rate: (c) voltage profiles and the corresponding XRD contour plots.

this electrolyte. Furthermore, electrochemical impedance spectroscopy (EIS) measurement was performed to display the resistance difference between the cells with these two electrolytes after one discharge step. As shown in Fig. S6, the Li || Gr cell with the DOL/DME electrolyte exhibits considerably larger resistance at high frequencies, which relates to the resistance at the SEI layer. This suggests that severe solvent reduction and other detrimental side reactions happened at the anode interphase, hampering Li⁺ diffusion.

Interestingly, differences in performance can also be observed in Li || Si/Gr cells with these two electrolytes, although a different lithiation mechanism (alloying with Li) is followed for the Si phase. 46 The cell utilizing the DOL/TTE electrolyte delivers notably higher specific capacities of 672 and 377 mA h g⁻¹, respectively, at the 1st and 80th cycle of a C/2 rate, compared to 463 and 273 mA h g⁻¹ for the DOL/DME cell (Fig. S7a). Moreover, the DOL/TTE cell shows an average CE of 99.5% over these 80 cycles compared to 98.2% for the DOL/DME cell. The inferior CE for the DOL/DME cell suggests that a significant amount of Li is consumed during the processes of SEI formation and electrolyte decomposition, especially during the first 20 cycles. Furthermore, voltage curves of the formation cycle and the 1st cycle at C/2 provide more details about the different behavior of the two electrolytes in Si/Gr cells (Fig. S7b and c). At the initial discharge step, the DOL/DME cell has a small voltage plateau, which may correspond to additional electrolyte decomposition at the anode or solvent intercalation as in the case of Gr anode. Meanwhile, the

DOL/DME cell has a clearly higher polarization at 341 mV for the 1st cycle at C/2 rate, compared to 227 mV for the DOL/TTE cell. This indicates that the SEI layer formed on the surface of the Si/Gr anode in the DOL/TTE electrolyte possesses lower resistance and higher ionic conductivity. Overall, these results prove that the DOL/TTE electrolyte shows promise with both the intercalation and non-intercalation type anodes, which can be further investigated in the future.

To better understand the structural change and reaction mechanisms of Gr anode during lithiation and delithiation, operando X-ray diffraction (XRD) measurements were conducted with Gr || Li configuration for both electrolytes (Fig. 2c and Fig. S8). Before cycling, a strong peak at 26.5° can be observed, corresponding to the interlayer diffraction peak (002) of pristine graphite. For the cell with DOL/DME electrolyte, the intensity of the graphite (002) peak significantly dropped as the cell started to discharge. However, the (002) peak corresponding to the stage-4/stage-3 intercalation phase did not show up in the first 10 hours when the cell voltage was above 0.25 V. Instead, a broad peak emerged at ~ 24° and persisted throughout the cycle, indicating a larger species entered the graphite interlayers. Meanwhile, the signals related to the LiC₆ and LiC₁₂ (stage-1/stage-2) phases were weak, as well as the graphite (002) peak after charging back. These phenomena confirm that Li* was not effectively intercalated into the graphite interlayers; on the contrary, solvent was likely co-intercalated with the solvated Li+, which triggered irreversible structural degradation of graphite. In sharp contrast, the cell with Materials Horizons COMMUNICATION

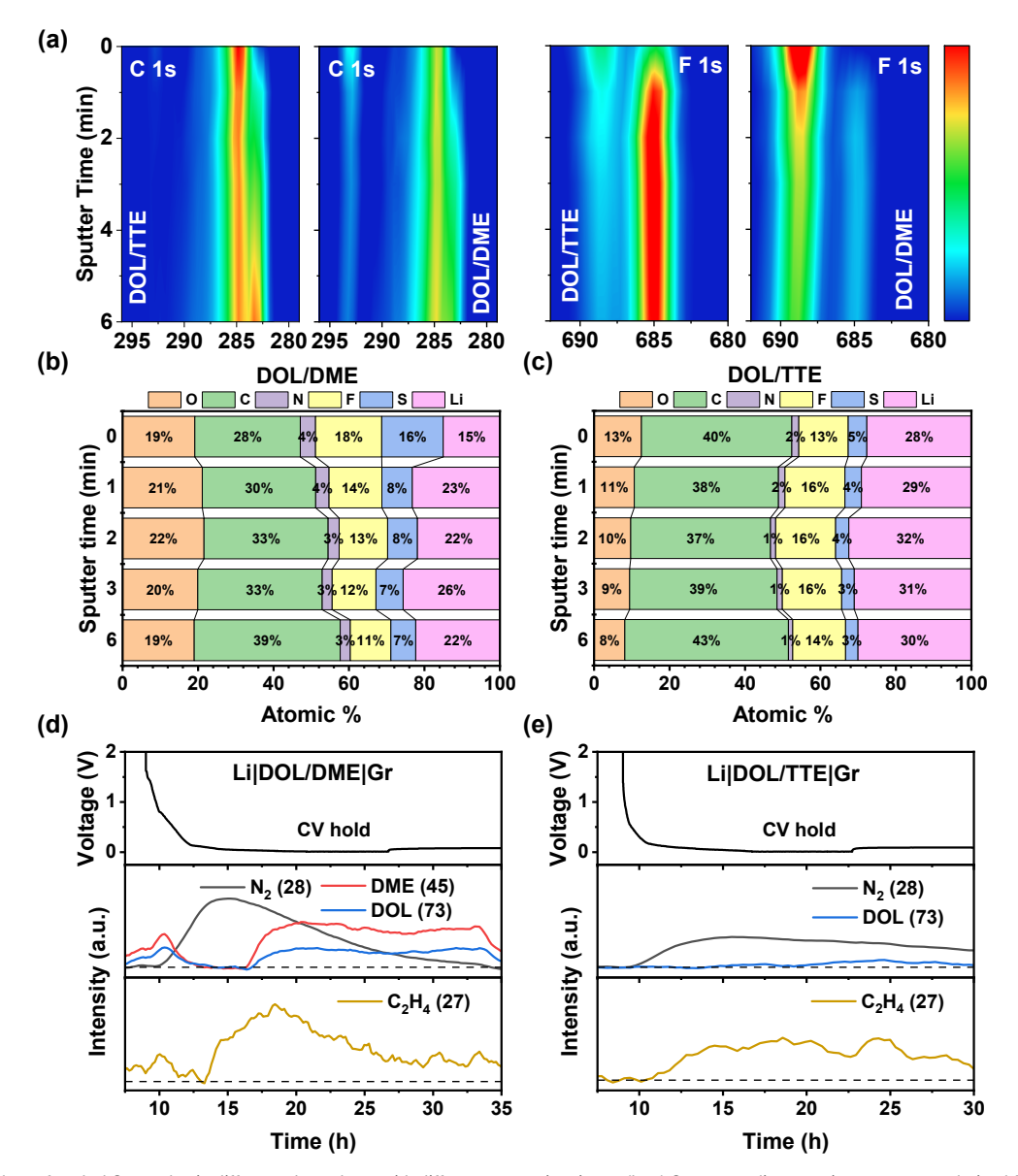


Fig. 3 (a) XPS data of cycled Gr anodes in different electrolytes with different sputtering times. (b, c) Corresponding atomic percentages derived from the XPS spectra. Voltage profiles (top) and the corresponding gas generation plots (bottom) for the Li || Gr cells with (d) DOL/TTE and (e) DOL/DME electrolytes. The number next to each species in the legends represents the m/z value of that curve. The black dashed line indicates the background curve (zero intensity).

DOL/TTE electrolyte showed strong (002) peaks for each intercalation phase during both discharge and charge, suggesting typical stage behaviors for Li intercalation and highly reversible phase transformation processes.^{47,48}

X-ray photoelectron spectroscopy (XPS) measurements were further performed on cycled Gr anodes to investigate the surface characteristics of the anodes with different electrolytes. As observed in C 1s and S 2p spectra, both anodes show species from solvent and salt decomposition (Fig. S9). Specifically, the C=O (~ 286.3 eV) and C-O (~ 289.0 eV) peaks in the C 1s spectra correspond to solvent decomposition, while the -SO₂ (~ 169.3 eV) and S-O (~ 167.4 eV) peaks in the S 2p spectra are from the TFSI anion and its decomposition products. However, the DOL/DME sample displays higher C-F peaks at ~ 293.1 eV in the C 1s spectrum

and at \sim 688.7 eV in the F 1s spectrum, which may be related to the organic species derived from reactions between the TFSI⁻ anions and intercalated solvent molecules in the Gr anode. In contrast, the DOL/TTE sample shows a strong Li-F peak at 685.0 eV, indicating the formation of LiF from anion decomposition without solvent degradation. This LiF-rich layer plays an important role in stabilizing the SEI structure. Moreover, in the O 1s spectra, the DOL/DME sample shows a stronger peak at \sim 533 eV compared to the DOL/TTE sample, which could be originating from the increased salt (LiTFSI and LiNO₃) and solvent decomposition.

Additionally, Ar-cluster sputtering was employed to better characterize the chemical composition closer to the bulk Gr. Note that this technique can reduce the surface reactions induced by the ion beam compared to regular Ar⁺

sputtering, thereby making the results more reliable. Atomic percentages were calculated from each spectrum collected with different sputtering times. For the DOL/DME sample, the C-F peaks persist during 6 min of sputtering, while the DOL/TTE sample has consistent Li-F signals, supporting the assumption that the intercalated solvent molecules may undergo decomposition in the bulk Gr (Fig. 3a). Meanwhile, the DOL/DME sample shows O, N, and S contents of 19.1%, 4.0%, and 16.3%, respectively, before sputtering, and 19.0%,2.7%, and 6.6%, respectively, after 6 min of sputtering, all significantly higher than those of the DOL/TTE sample (Fig. 3b and c). Based on their binding energies, they are mostly O/N/F-containing organic species and oxidized sulfur species from solvent and salt decompositions. These results, along with the fact that the DOL/TTE sample has lower C-O/C-C ratios, confirm the formation of a less organic SEI layer with less detrimental electrolyte decomposition for the DOL/TTE sample (Fig. S10). Moreover, the residual LiC_x peaks at 283 eV appeared later for the DOL/DME sample and were not as strong as those for the DOL/TTE sample, suggesting that the SEI layer was thicker and Li⁺ was not effectively intercalated into Gr layers for the anodes cycled in DOL/DME.

Off-gassing behavior during cycling is another important metric determining the stability of an electrolyte. 49,50 Here, online electrochemical mass spectroscopy (OEMS) was utilized to monitor real-time gas generation during the operation of the Gr || Li cells with different electrolytes (Fig. 3d and e). The cells underwent one discharge step with constant voltage hold followed by a rest period. At the

beginning of the discharge, signals corresponding to DOL and DME could be detected for the DOL/DME cell. The timing aligns well with the solvent co-intercalation as we discussed before, indicating possible release and decomposition of the solvent molecules along with their co-intercalation. The offgassing rates of DOL and DME dropped when the voltage was below ~ 0.15 V, while a significant amount of N_2 gas started to be generated. This may originate from the reduction of TFSI⁻ anions during the SEI formation. As the voltage became lower, there was more DOL and DME being released, again accompanied by the generation of C2H4, probably due to the increased amount of solvent reduction at the anode. 48 NO and NO2 could also be detected in the DOL/DME cell, corresponding to the decomposition of LiNO₃ (Fig. S11). Interestingly, the evolution of these two gases follows a similar pattern with DOL and DME, suggesting that the reduction of LiNO₃ and its off-gassing behavior may also closely relate to the solvent co-intercalation and reduction process at the anode. Compared to the DOL/DME cell, no obvious solvent signals and weaker N_2 and C_2H_4 signals could be detected in the DOL/TTE cell, confirming that the solvent reduction and off-gassing are effectively inhibited.

In fact, the DOL/TTE electrolyte exhibits good compatibility with both the Gr anode and sulfur cathode, which helps to unleash the advantage of Gr anode in the cyclability. Fig. 4a compares the long-term cycling performance of Li-S cells with either Li-metal or Gr anode, utilizing DOL/TTE electrolyte. The Gr anode was electrochemically pre-lithiated before pairing with a sulfur cathode. The cell with lithiated-Gr (Li-Gr) anode shows an

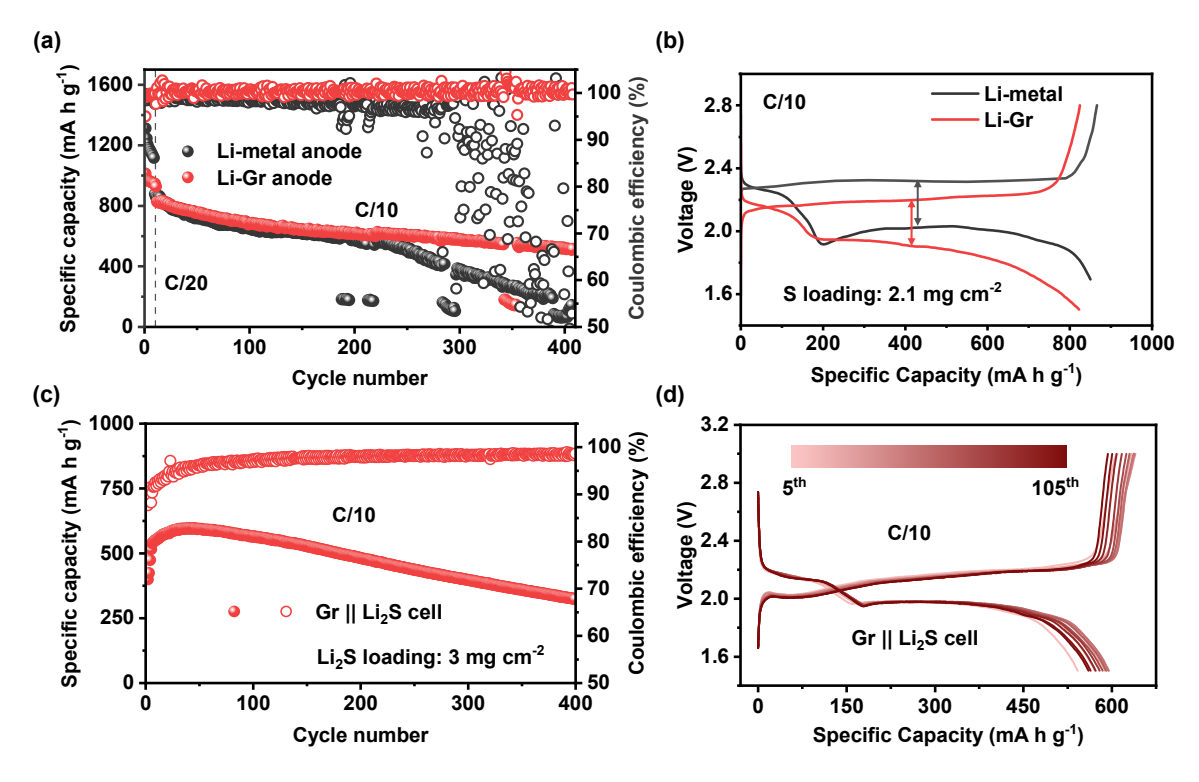


Fig. 4 (a) Cycling performance of Li-S cells with Li-metal anode and Li-Gr anode in the DOL/TTE electrolyte; (b) corresponding voltage profiles of the 2^{nd} cycle at C/10 rate. (c) Cycling performance of Gr || Li₂S full cell in DOL/TTE electrolyte; (d) corresponding voltage profiles of the 5^{th} – 105^{th} cycles (every 10 cycles).

Materials Horizons COMMUNICATION

initial discharge capacity of 826 mA h g⁻¹ and retains 62.3% of it (515 mA h g⁻¹) after 400 cycles at C/10 rate. The cell with Li-metal anode, although having a similar initial capacity of 878 mA h g⁻¹, has a capacity retention of only 16.3%, primarily due to rapid Li metal failure after 250 cycles. Meanwhile, the Li-Gr anode cell has stable CEs over 400 cycles with an average of 99.6%, contrasting lower and fluctuating values for the Li-metal anode cell. It should be noted that an excess amount of Li metal was employed in the Li || S cell (N/P \approx 20), while the Li-Gr || S cell has an N/P ratio of 1.5. These results suggest that, with a suitable electrolyte like DOL/TTE, Gr anode can be applied into Li-S cells to reduce anode degradation and enable superior long-term cycling performance. Additionally, the voltage profile of the Li-Gr anode cell shows a ~ 0.1 V decrease compared to the Li-metal cell due to the potential difference between Gr and Li metal, while the overpotential remains similar (~ 290 mV, Fig. 4b). This indicates that Gr anode has little effect on the cathode reaction chemistry and kinetics. Rate performance of the Li-Gr anode cell was also evaluated. As shown in Fig. S12, the cell exhibits a reversible capacity of 625 mA h g⁻¹ at C/2 rate, indicating sufficient conversion kinetics at the sulfur cathode.

Furthermore, to evaluate the cell performance with an even lower N/P ratio, Gr || Li₂S full cells were assembled. By utilizing Li₂S as the cathode active material, Gr anode can be used as it is without pre-lithiation because the Li₂S cathode is in a fully lithiated state. Meanwhile, Li₂S cathode can ameliorate the volume expansion issues encountered with regular sulfur cathode, making this a promising configuration for the Li-S system. Here, an N/P ratio of 1.05 was used, and the electrochemical cycling performance was tested at C/10 rate. The Gr || Li₂S cell with DOL/TTE electrolyte underwent an initial activation stage when the capacity gradually increased, due to the slow activation of Li₂S (Fig. 4c). The cell was able to retain a capacity of 257 mA h g-1 after 400 cycles, corresponding to 369 mA h g-1 if calculated by per gram of sulfur. Moreover, charge and discharge voltage profiles of the Gr || Li₂S cell exhibit stable overpotentials and capacities from the 5th to 105th cycles (Fig. 4d). The electrochemical performance data indicate that DOL/TTE electrolyte can support stable cycling of Li-S full cells with Granode and Li₂S cathode, due to its compatibility with both the electrodes and ability to suppress detrimental LiPS shuttling.

3. Conclusion

In summary, we have developed an optimized ether electrolyte (1 M LiTFSI in DOL/TTE) to enable the use of Grbased anodes in Li-S batteries. By tuning the solvation structure, the Li⁺ de-solvation energy was reduced, thereby suppressing the solvent co-intercalation and enabling a stable cycling of Gr anodes. The DOL/TTE electrolyte favored the formation of a thinner and more inorganic SEI layer. Additionally, this electrolyte suppressed the detrimental gas generation from electrolyte decomposition compared to a

conventional dilute ether electrolyte. As a proof of concept, similar performance improvements were also observed in Si/Gr anodes. Meanwhile, at the cathode, the DOL/TTE electrolyte reduced the solubility of LiPS while maintaining sufficient conversion kinetics, allowing for stable cycling without cathode modification. The Li-Gr|| sulfur cell showed better long-term cyclability, even with a lower N/P ratio, compared to the Li-metal cell. Furthermore, a Gr || Li₂S full cell demonstrated over 400 cycles with an N/P ratio of 1.05 and a Li₂S loading of 3 mg cm⁻². In all, this work showcases a rational approach to utilizing non-Li-metal anodes in Li-S batteries with ether-based electrolytes, paving the way for their practical application.

Author contributions

Tianxing Lai: conceptualization, investigation, visualization, writing – original draft; Amruth Bhargav: conceptualization, investigation, writing – review & editing; Seth Reed: investigation, formal analysis; Arumugam Manthiram: conceptualization, funding acquisition, supervision, writing – review & editing.

Conflicts of interest

There are no conflicts of interest to declare.

Data availability

The data supporting this article have been included as part of the Supplementary Information.

Acknowledgements

This work was supported by the U.S. Department of Energy, Office of Basic Energy Sciences, Division of Materials Science and Engineering under award number DE-SC0005397.

References

- W. Yao, K. Liao, T. Lai, H. Sul and A. Manthiram, Chem. Rev., 2024, 124, 4935-5118.
- C. Bi, Y. Zhu, Z. Li, M. Zhao, X. Zhang, B. Li and J. Huang, *Adv. Energy Mater.*, 2024, n/a, 2402609.
- 3 Z. Chen, Q. Cheng, X. Li, Z. Li, Y. Song, F. Sun, M. Zhao, X. Zhang, B. Li and J. Huang, J. Am. Chem. Soc., 2023, 145, 16449-16457.
- 4 T. Lai and A. Manthiram, *Adv. Funct. Mater.*, 2024, DOL: 10.1002/adfm.202405814.
- 5 B. Jin, T. Lai and A. Manthiram, *ACS Energy Lett.*, 2023, **8**, 3767-3774.
- 6 Y. Zhao, X. Zheng, P. Gao and H. Li, *Mater. Horiz.*, 2023, **10**, 3948-3999.
- 7 C. Y. Kung and S. H. Chung, *Mater. Horiz.*, 2023, **10**, 4857-4867.
- 8 K. Liao, A. Bhargav and A. Manthiram, *ACS Appl. Energ. Mater.*, 2023, **6**, 9585-9593.

- 9 Y. He, X. Jing, T. Lai, D. Jiang, C. Wan, P. S. Postnikov, O. Guselnikova, L. Xu, X. He, Y. Yamauchi and B. Jin, J. Mater. Chem. A, 2024, 12, 12681-12690.
- 10 X. Dong, X. Liu, P. K. Shen and J. Zhu, *Adv. Funct. Mater.*, 2023, **33**, 2210987.
- 11 A. Rafie, R. Pai and V. Kalra, J. Mater. Chem. A, 2021, 9, 26976-26988.
- 12 B. Jin, L. Yang, J. Zhang, Y. Cai, J. Zhu, J. Lu, Y. Hou, Q. He, H. Xing, X. Zhan, F. Chen and Q. Zhang, Adv. Energy Mater., 2019, 9.
- 13 X. Cheng, J. Huang and Q. Zhang, *J. Electrochem. Soc.*, 2017, **165**, A6058-A6072.
- 14 T. Lai, A. Bhargav and A. Manthiram, *Adv. Funct. Mater.*, 2023, **33**, 2304568.
- 15 Y. Yen and A. Manthiram, ACS Appl. Mater. Interfaces, 2024, **16**, 34997-35005.
- 16 Y. Wu, C. Wang, C. Wang, Y. Zhang, J. Liu, Y. Jin, H. Wang and Q. Zhang, *Mater. Horiz.*, 2024, **11**, 388-407.
- 17 Z. Zhao, B. Nian, Y. Lei, L. Zhao, M. N. Hedhili, D. Guo, Z. Shi, W. Zhao, J. K. El-Demellawi, Y. Wang, Y. Zhu, K. Xu and H. N. Alshareef, *Adv. Mater.*, 2024, **n/a**, 2402626.
- 18 X. Cao, H. Jia, W. Xu and J. Zhang, *J. Electrochem. Soc.*, 2021, **168**, 10522.
- 19 Z. Guo, Z. Cui, R. Sim and A. Manthiram, *Small*, 2023, **19**, 2305055.
- 20 M. Pai, T. Lai and A. Manthiram, Adv. Funct. Mater., 2024, n/a, 2407450.
- 21 Q. Miao, N. Solan, G. Hyun, J. Holoubek and P. Liu, *ACS Energy Lett.*, 2023, **8**, 4818-4830.
- 22 L. Su, N. Yao, Z. Li, C. Bi, Z. Chen, X. Chen, B. Li, X. Zhang and J. Huang, *Angew. Chem., Int. Ed.*, 2024, **63**, e202318785.
- 23 X. Li, S. Feng, Y. Song, C. Zhao, Z. Li, Z. Chen, Q. Cheng, X. Chen, X. Zhang, B. Li, J. Huang and Q. Zhang, *J. Am. Chem. Soc.*, 2024, **146**, 14754-14764.
- 24 Z. Li, L. Hou, N. Yao, X. Li, Z. Chen, X. Chen, X. Zhang, B. Li and Q. Zhang, *Angew. Chem.*, *Int. Ed.*, 2023, **62**, e202309968.
- 25 Z. Jiang, Z. Zeng, W. Hu, Z. Han, S. Cheng and J. Xie, Energy Storage Mater., 2021, 36, 333-340.
- 26 B. Jin, A. Dolocan, C. Liu, Z. Cui and A. Manthiram, *Angew. Chem.*, *Int. Ed.*, 2024, **n/a**, e202408021.
- 27 A. Manthiram, Nat. Commun., 2020, 11, 1550.
- 28 J. Ming, Z. Cao, W. Wahyudi, M. Li, P. Kumar, Y. Wu, J. Hwang, M. N. Hedhili, L. Cavallo, Y. Sun and L. Li, ACS Energy Lett., 2018, 3, 335-340.
- 29 J. Zhang, Q. Fu, P. Li, R. Linghu, X. Fan, H. Lin, J. Bian, S. Han, G. Sun and L. Kong, *Particuology*, 2024, **89**, 238-245.
- 30 J. Zhang, X. Fan, X. Zhou, R. Hu, N. Du, C. Guan, S. Han, B. Li and L. Kong, *Energy Storage Mater.*, 2024, **73**, 103786.
- 31 T. Yim, M. Park, J. Yu, K. J. Kim, K. Y. Im, J. Kim, G. Jeong, Y. N. Jo, S. Woo, K. S. Kang, I. Lee and Y. Kim, *Electrochim. Acta*, 2013, **107**, 454-460.
- 32 D. Xia, E. P. Kamphaus, A. Hu, S. Hwang, L. Tao, S. Sainio, D. Nordlund, Y. Fu, H. Huang, L. Cheng and F. Lin, *ACS Energy Lett.*, 2023, **8**, 1379-1389.
- 33 A. Bhargav, M. Wu and Y. Fu, *J. Electrochem. Soc.*, 2016, **163**, A1543-A1549.
- 34 S. Chen, Z. Yu, M. L. Gordin, R. Yi, J. Song and D. Wang, ACS Appl. Mater. Interfaces, 2017, 9, 6959-6966.
- 35 L. L. Jiang, C. Yan, Y. X. Yao, W. Cai, J. Q. Huang and Q. Zhang, *Angew. Chem.*, *Int. Ed.*, 2021, **60**, 3402-3406.
- 36 P. Zeng, Y. Han, X. Duan, G. Jia, L. Huang and Y. Chen, *Mater. Res. Bull.*, 2017, **95**, 61-70.
- 37 D. Huang, Z. Wang, R. Han, S. Hu, J. Xue, Y. Wei, H. Song, Y. Liu, J. Xu, J. Ge and X. Wu, Adv. Sci., 2023, 10, 2302966.

- 38 F. S. Hoffmann, F. Schmidt, J. Müller, K. Schönherr, S. Dörfler, T. Abendroth, H. Althues, A. Kwade, N. L. Wu and S. Kaskel, *Batteries Supercaps*, 2023, **6**, e202300093.
- 39 M. Qin, Z. Zeng, Q. Wu, H. Yan, M. Liu, Y. Wu, H. Zhang, S. Lei, S. Cheng and J. Xie, *Energy Environ. Sci.*, 2023, **16**, 546-556.
- 40 J. Holoubek, H. Liu, Z. Wu, Y. Yin, X. Xing, G. Cai, S. Yu, H. Zhou, T. A. Pascal, Z. Chen and P. Liu, *Nat. Energy*, 2021, 2021, 303-313.
- 41 D. M. Seo, O. Borodin, S. Han, P. D. Boyle and W. A. Henderson, J. Electrochem. Soc., 2012, 159, A1489-Δ1500
- 42 Y. Yamada, K. Furukawa, K. Sodeyama, K. Kikuchi, M. Yaegashi, Y. Tateyama and A. Yamada, *J. Am. Chem. Soc.*, 2014, **136**, 5039-5046.
- 43 J. Tan, M. Ye and J. Shen, *Mater. Horiz.*, 2022, **9**, 2325-2334.
- 44 W. Wahyudi, V. Ladelta, L. Tsetseris, M. M. Alsabban, X. Guo, E. Yengel, H. Faber, B. Adilbekova, A. Seitkhan, A. Emwas, M. N. Hedhili, L. Li, V. Tung, N. Hadjichristidis, T. D. Anthopoulos and J. Ming, *Adv. Funct. Mater.*, 2021, 31, 2101593.
- 45 P. Ma, P. Mirmira, P. J. Eng, S. Son, I. D. Bloom, A. S. Filatov and C. V. Amanchukwu, *Energy Environ. Sci.*, 2022, **15**, 4823-4835.
- 46 M. T. McDowell, S. W. Lee, W. D. Nix and Y. Cui, *Adv. Mater.*, 2013, **25**, 4966-4985.
- 47 C. Weisenberger, D. K. Harrison, C. Zhou and V. Knoblauch, *Electrochim. Acta*, 2023, **461**, 142629.
- 48 M. Winter, J. O. Besenhard, M. E. Spahr and P. Novák, *Adv. Mater.*, 1998, **10**, 725-763.
- 49 R. Bernhard, M. Metzger and H. A. Gasteiger, *J. Electrochem. Soc.*, 2015, **162**, A1984-A1989.
- 50 A. Jozwiuk, B. B. Berkes, T. Weiss, H. Sommer, J. Janek and T. Brezesinski, *Energy Environ*. *Sci.*, 2016, **9**, 2603-2608.

Data Availability Statement

The datasets generated during and/or analyzed during the current study are available from the authors on reasonable request.